The infrared absorption spectrum of radioactive water isotopologue $H_2{}^{15}O$

Boris A. Voronin[a,b], Jonathan Tennyson[c,*], Sergey N. Yurchenko[c], Tatyana Yu. Chesnokova[b], Aleksei V. Chentsov[b], Aleksandr D. Bykov[b], Maria V. Makarova[d], Svetlana S. Voronina[b], Flávio C. Cruz[a]

[a] *Instituto de Fisica Gleb Wataghin, Universidade Estadual de Campinas, Campinas, SP, 13083-859, Brazil*
[b] *V.E. Zuev Institute of Atmospheric Optics SB RAS, sq. Ak. Zuev 1, 643021 Tomsk, Russia*
[c] *Department of Physics and Astronomy, University College London, Gower Street, London WC1E 6BT, UK*
[d] *Faculty of Physics, St. Petersburg State University, 198504 St. Petersburg, Russia*

Abstract

A room temperature line list for the $H_2{}^{15}O$ radioactive isotopologue of the water molecule is computed using the variational nuclear-motion DVR3D program suite and an empirical high-precision potential energy function. The line list consists of rotation-vibrational energies and Einstein-A coefficients, covering a wide spectral range from 0 to 25000 cm^{-1} and the total angular momenta J up to 30. Estimates of air-broadening coefficients are provided. Experimentally derived energies of $H_2{}^{16}O$, $H_2{}^{17}O$ and $H_2{}^{18}O$ from the literature are used to provide improvied energies for important states with uncertainty estimates for the $H_2{}^{15}O$. A number of most promising spectroscopic ranges for the detection of $H_2{}^{15}O$ are proposed. The calculated absorption spectrum should be useful for the study gaseous radioactive water at IR region, determining concentration, etc.

Keywords:

$H_2{}^{15}O$, energy levels, water vapor, absorption lines, line shape parameters, VoTe-15

1. Introduction

The water molecule is the most common triatomic molecule in the Universe. Water is the major absorber of both incoming and outgoing radiation in the Earth's atmosphere; it is arguably the most important species for both life on Earth in general and for humans in particular. Unsurprisingly therefore H_2O is one of the most well studied molecules.

*Corresponding author.
Email address: j.tennyson@ucl.ac.uk (Jonathan Tennyson)

In addition to the parent isotopologue of water, $H_2{}^{16}O$, more than 500 of other isotopologues of the water molecule are possible [1], combined from 7 isotopes of hydrogen H - ^{1}H, ^{2}H (D- deuterium), ^{3}H (T- tritium), ^{4}H, ^{5}H, ^{6}H, ^{7}H [2, 3] and a large number of the oxygen isotopes, from ^{11}O[4] to ^{28}O [5]. Starting from ^{3}H , the hydrogen isotopes are radioactive, starting from ^{4}H they are ultra-short-lived. Out of 17 isotopes of oxygen, only 3 are stable – ^{16}O, ^{17}O, and ^{18}O; the others are all radioactive. Of the radioactive oxygen isotopes, the longest-lived species is ^{15}O, whose half-life exceeds 2 minutes. Conversely, tritium has a half-life of more than 12 years and spectra of the tritium enhanced water have been observed, see e.g. [6], both for $HT^{16}O$ and $T_2{}^{16}O$. In addition, calculated spectra of various tritium isotopologues of water can be found in the spectroscopic database spectra.iao.ru [7].

The $H_2{}^{15}O$ water isotopologue has been used for many decades in biological and medical research, [8–13] , but its infrared (IR) spectrum has yet to be observed. Therefore, at present the source of the spectroscopic information on $H_2{}^{15}O$ is only through theory [14]. The measurement of spectra of short-lived radioactive isotopologues is associated with significant technical problems. However, calculations such as the ones presented here facilitate the measurement and interpretation of such spectra. Any theoretical calculation should be adapted from one which reproduces the measured spectra of the parent $H_2{}^{16}O$ and other known isotopologues of water. For this purpose, several approaches will be used in this work, which are described below.

Studying the spectrum of unstable water isotopologues can be useful for solving a number of scientific and technical problems. For example, the study of the properties of water in liquid or gaseous states irradiated by hard gamma radiation, to study nuclear processes in the atmosphere during a thunderstorm, in positron tomography etc. (see, for example, [15–21]). A partial absorption spectrum of of $H_2{}^{15}O$ calculated by us for transitions up to $J = 10$ was recently presented by Voronin et al. [14] and a number of vibrational energy levels of $H_2{}^{15}O$ as well as of all other radioactive oxygen isotopes of water were published by Voronin and Bykov [1].

This paper presents a theoretical line list for $H_2{}^{15}O$ obtained via a direct variational calculation up to J=30 using a high accuracy potential energy surface (PES) from Bubukina et al. [22], a dipole moment surface (DMS) from Lodi et al. [23] and the accurate variational software package DVR3D [24]. DVR3D has been used to produce a number of high accuracy line list for H_2O and its isotopologues including BT2 [24], VTT [25], POKAZATEL [26], Conway [27], HotWat78 [28], VoTe [29, 30] as well as for many other triatomic molecules. In our recent work [14], a tentative

detection of a transient $H_2{}^{15}O$ line from atmospheric measurement taken after thunderstorms was presented with an absorption feature at 1973.5 cm^{-1}. In this work we provide a more detailed analysis of this feature and use available empirical energy levels for $H_2{}^{16}O$, $H_2{}^{17}O$ and $H_2{}^{18}O$ to provide reliable energy levels and hence transitions wavenumbers for $H_2{}^{15}O$; we suggest a number of promising spectroscopic regions for possible detections of $H_2{}^{15}O$.

There are a number of works that show how to use experimental and theoretical data of known, more abundant isotopologues for predicting energies of the less abundant species [31–41]. Here we explore some of the ideas from the literature to provide the uncertainty estimates for the calculated energies of $H_2{}^{15}O$ as well as pseudo-experimental corrections.

.

2. Calculated line list for $H_2{}^{15}O$

Here we follow the same calculation procedure as in Voronin et al. [14] to produce a room temperature line list for $H_2{}^{15}O$ covering the rotational excitation up to J=30.

The calculations were carried out as follows. At the first stage, the ro-vibrational energy levels and wave functions of $H_2{}^{15}O$ were calculated with the DVR3D variational nuclear motion program [24] using an empirical PES from Bubukina et al. [22] and an *ab initio* dipole moment surface (DMS) from Lodi et al. [23]. The PES by Bubukina et al. [22] was obtained by fitting its Born-Oppenheimer contribution to experimental energies of $H_2{}^{16}O$ while the mass dependence was included through an adiabatic (DBOC) term developed by Partridge and Schwenke [42]. Here we switch to $H_2{}^{15}O$ by changing the mass of ^{16}O to ^{15}O, for which used a value of 15.0030656 Da [43]. The variation in energy corresponding to isotopic substitution of the heavier atom O is relatively small, but not negligible as far as the high-resolution spectroscopy applications are concerned. The accuracy of the PES and the whole procedure for calculations of spectra of isotopologues has been demonstrated in Polyansky et al. [40], where accurate line lists for $H_2{}^{17}O$ and $H_2{}^{18}O$ were presented. We note that analysis by Császár et al. [44] suggests that the equilibrium geometry will change very little between the various $H_2{}^{X}O$ isotopologues, and while calculations have predicted some non-Born-Oppenheimer behaviour of the dipole moment [45], this will only be a minor contribution for strong transitions which are the only ones likely to be observable for $H_2{}^{15}O$.

The computations were performed on the computer cluster “amun” at UCL as well as on workstations in the V.E. Zuev IAO SB RAS and the Gleb Watagin Institute of Physics (Campinas,

Brazil). The final line list of $H_2{}^{15}O$ comprises a total of 149,665,544 (almost one hundred and fifty million) transitions.

3. Energy levels of $H_2{}^{15}O$

No spectroscopic measurements of $H_2{}^{15}O$ exist and it is therefore difficult to assess the quality of our calculations directly. Indirectly, one can take the advantage of the wealth of the spectroscopic information on the $H_2{}^{16}O$, $H_2{}^{17}O$ and $H_2{}^{18}O$ water isotopologues as collected in the W2020 compilation of experimentally derived energies of water [46]. W2020 contains 19225 energy levels ($J_{\max}$=42) of $H_2{}^{16}O$, 5278 energy levels ($J_{\max}$=20) of $H_2{}^{17}O$ and 6865 energy levels ($J_{\max}$=20) of $H_2{}^{18}O$, all uniquely assigned the ro-vibrational quantum numbers (v_1 v_2 v_3) [J K_a K_c]. It should be noted that the common states between the $H_2{}^{17}O$ and $H_2{}^{18}O$ sets are only for $J \leq 19$.

For our analysis we could identify 4622 common levels in these three sets that belong to the same states, i.e. with the same quantum numbers. As an example, Fig. 1(left) illustrates the generally well-behaved correspondence between ro-vibrational energies of $H_2{}^{16}O$ and $H_2{}^{18}O$ by showing the energy difference for the vibrational state ν_1 (100) as a function of J, where the dependence on J is nice and smooth.

It should be also noted, that when comparing these three sets to each other, clear outliers with unusually large differences between same state energies of $H_2{}^{X}O$, X=16,17,18 were identified, see Table 1. This is illustrated for $5\nu_1$ in Fig 1(right), where outliers can clearly be seen. It should be noted that such isotopologue analysis is a useful tool to identify inconsistent or wrong assignments, as e.g. shown in Table 1 for the $5\nu_1$ state, see also the work by Viglaska-Aflalo et al. [41]. Accidental resonances are a common occurrence in molecular spectra which also cause the behavior between isotopologues to appear erratic. For example, in water resonances can arise due to the appearance of transitions with a large value of v_2 [47, 48]; such resonances not only cause shifts in line position but also cause problems with labeling which can become rather arbitrary when states are heavily mixed.

In order to estimate the accuracy of the DVR3D energies of $H_2{}^{15}O$, we used the same PES by Bubukina et al. [22] and computed ro-vibrational energies of the $H_2{}^{X}O$, X= 17, 18 isotopologues up to J=20. The corresponding masses of oxygen were taken as 16.99913175595 for ^{17}O and 17.99915961214 for ^{18}O [43]. For simplicity, hereinafter these calculations are be referred to as VoTe-17 and VoTe-18 to distinguish them from the original VoTe [29, 30] calculation for $H_2{}^{16}O$.

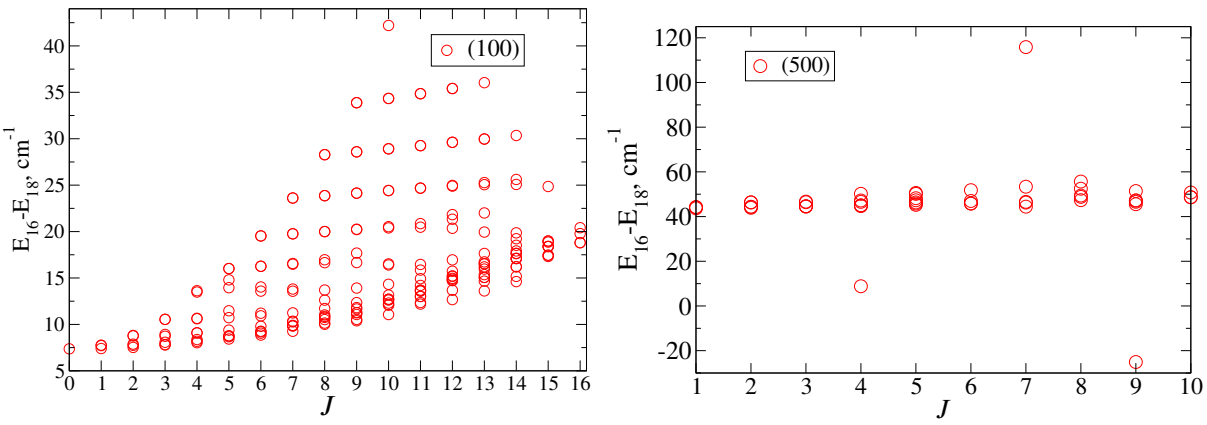

Figure (1) Differences between the same vibration state rotational energy levels of $H_2{}^{16}O$ and $H_2{}^{18}O$: Left: the (100) vibration state; Right: the (500) vibrational state.

The lower energy value in the calculation for $H_2{}^{17}O$ water is 5412.19011825 cm^{-1}, and for $H_2{}^{18}O$ water is 5405.16727619 cm^{-1}. Here we compare these results for the selected set of the experimental 4620 energies of $H_2{}^{X}O$, X=17,18 from W2020 to check and hopefully improve the $H_2{}^{15}O$ DVR3D energies below.

3.1. Comparison of the DVR3D (VoTe, VoTe−17 and VoTe−18) and W2020 energy energy levels of $H_2{}^{16}O$, $H_2{}^{17}O$ and $H_2{}^{18}O$

3.1.1. $H_2{}^{16}O$

Let us first establish the agreement between theory and experiment for the main isotopologue. We can use the experimental energy levels of $H_2{}^{16}O$ fro the W2020 work [46] (19225 values) to compare to the theoretical VoTe $H_2{}^{16}O$ energies [30] computed with the PES by Bubukina et al. [22]. Although in principle, W2020 extends up to ∼41143.77 cm^{-1} (the highest level is (16 3 30) [1 1 1] and up to the rotational quantum number J of 42, such high energies beyond the scope of this study.

Here we select only states below 25000 cm^{-1}. We also exclude a few potential outliers exhibiting large differences of up to 2.5 cm^{-1} between the VoTe and W2020 values, which can be caused by a number of reasons including calculation errors, problems in the W2020 compilation or strong resonances not properly accounted for by the PES.

As a result, a set of 18512 energy levels of $H_2{}^{16}O$ was compiled. For this set root-mean-squares (RMS) error ($\sqrt{\sum_i (E_i^{\rm obs} - E_i^{\rm calc})^2/N}$) is 0.1335 cm^{-1} and the maximal deviation is 2.16 cm^{-1}.

Reducing this set to those levels within 1 cm^{-1} of each other gives an average absolute difference of 0.07598 cm^{-1} and an RMS error of 0.1267 cm^{-1} for 18494 levels, while reduction to within 0.1

cm^{-1}gives an RMS error of 0.03940 cm^{-1} for 13903 levels.

3.1.2. $H_2{}^{17}O$

Now we turn to $H_2{}^{17}O$ and compare the calculated VoTe-17 energies to the corresponding experimental values in W2020. For $H_2{}^{17}O$, there are 5278 energy levels in W2020 with the maximal energy value of 18396 $cm^{-1}$and maximal rotational quantum number J of 20. Out of 5278 states, two levels could not be matched to VoTe-17. For this set of 5276 levels of $H_2{}^{17}O$, the difference between W2020 and VoTe-17 gives the RMS error of 0.1463 cm^{-1}.

The comparison between 5276 W2020 levels and VoTe-17 is key for our study as we will use it to estimate the error of our $H_2{}^{15}O$ ro-vibrational energies as, like $H_2{}^{15}O$, $H_2{}^{17}O$ is just one unit mass different from $H_2{}^{16}O$ and we therefore expect that the errors arising from energy estimates due to isotopic substitution should be similar.

3.1.3. $H_2{}^{18}O$

For $H_2{}^{18}O$ there are 6865 energy levels in W2020 [46] ranging up to 18396 cm^{-1} J=20, which were selected for the analysis. The obs.-calc. error of the calculated VoTe-18 energies from W2020 range from -1.5 cm^{-1} to 1.8 cm^{-1} with the RMS error of 0.1513 cm^{-1}.

3.2. Sets of levels for different comparisons.

As was mentioned above, we initially selected 4620 sets of energies of $H_2{}^{16}O$, $H_2{}^{17}O$ and $H_2{}^{18}O$ from W2020 for the analysis that shared the same quantum numbers. Out of these 4620 state, 61 states could not be matched to the VoTe levels using the theoretical assignment of the latter from [30]. Some states were also excluded if the rule $E_{15} > E_{16} > E_{17} > E_{18}$ was violated or the difference between energies of the isotopologues was too high (> 200 cm^{-1}). This resulted in 4440 states for which all three experimental W2020 sets ($H_2{}^{16}O$, $H_2{}^{17}O$ and $H_2{}^{18}O$) as well as the three theoretical sets (VoTe, VoTe-17 and VoTe-18) could be all mutually correlated.

For the majority (4127) of the selected states the difference between the theory and experiment is found to lie within 5 cm^{-1}, while 3934 levels had residuals within 1 cm^{-1}. Some outliers had differences up to 10 cm^{-1} (e.g. -13.18 cm^{-1} for the state (021) [717] of $H_2{}^{16}O$), 20 cm^{-1} (e.g. $+20.02$ cm^{-1} for the state (420) [717] of $H_2{}^{16}O$) or even $+37.22$ cm^{-1} for the state (101) [16 0 16] of $H_2{}^{16}O$. Such unusually large outliers are most likely due to misassignment problems either in the theoretical or experimental sets or both. We therefore excluded states that exhibit large differences between the theoretical energies and those from W2020 using a threshold of 5 cm^{-1}, which resulted

in a set of 4127 common states. For a more stringent selection, we will also use a set of 3934 states whose differences from experiment do not exceed 1 cm^{-1} or a set of 3426 levels whose differences are within 0.1 cm^{-1}. This is illustrated in Figs. 2, where the obs.-calc. residuals between the w2020 and VoTe data sets for $H_2{}^{17}O$ and $H_2{}^{18}O$ are shown.

Since the PES of Bubukina et al. [22] was originally obtained by fitting to the ro-vibrational energies of $H_2{}^{16}O$ only, we need to establish the errors introduced when using it for other isotopologues. For $H_2{}^{18}O$ and $H_2{}^{17}O$ this can be readily done by comparing to the W2020 'experimental' energies, while for $H_2{}^{15}O$, with no experimental data at hand, we will assume that the errors in calculating the $H_2{}^{18}O$ and $H_2{}^{17}O$ energies are representative also for our $H_2{}^{15}O$ calculations. Moreover, for the $H_2{}^{15}O$ line list introduced below, the errors obtained for $H_2{}^{17}O$ will be considered to be reasonable indicators of the errors in the $H_2{}^{15}O$ calculations and used to estimate the corresponding uncertainties of $H_2{}^{15}O$, where such comparisons for $H_2{}^{17}O$ are available.

For the 4127 levels of VoTe-17, the calculated RMS error from the W2020 energy set is 0.2605 cm^{-1}. Note that the corresponding RMS error for VoTe-18 is increased to 0.6651 cm^{-1}, which is to be expected for the isotopologue $H_2{}^{18}O$ with its larger mass difference. This can be compared to the RMS error of 0.1256 cm^{-1} of the main isotopologue.

3.3. Isotopologue pseudo-experimental corrections

Following the pseudo-experimental extrapolation method proposed by Polyansky et al. [28], here we use the obs.-calc. residuals for the main isotopolgue to obtain empirical corrections to the ro-vibrational energy values of the minor isotopologues of water as follows :

$$E_N^{\rm corr} = E_N^{\rm calc} + E_{16}^{\rm obs} - E_{16}^{\rm calc}, \tag{1}$$

where $E_N^{\rm calc}$ is a DVR3D energy calculated for a minor isotopolue, $N = 15, 17, 18$, and $E_{16}^{\rm obs} - E_{16}^{\rm cacl}$ is an empirical correction estimated as the difference between the calculated and experimental energies of the parent (^{16}O) molecule. The approach, which has also been referred to as isotopologue-extrapolation (IE) [49], is based on the assumption that the main source of the error is from the inaccuracy of the Born-Oppenheimer PES of water, which should affect all four isotopologues similarly and was shown to work well for $H_2{}^{18}O$ and $H_2{}^{17}O$ [28]. Following Polyansky et al. [28], we will refer to $E_{16}^{\rm obs} - E_{16}^{\rm cacl}$ as the pseudo-experimental correction $E_N^{\rm corr}$.

In order to evaluate the accuracy of the pseudo-experimental corrections for $H_2{}^{15}O$, we carried out this procedure for the VoTe-17 and VoTe-18 sets and performed subsequent evaluation of the

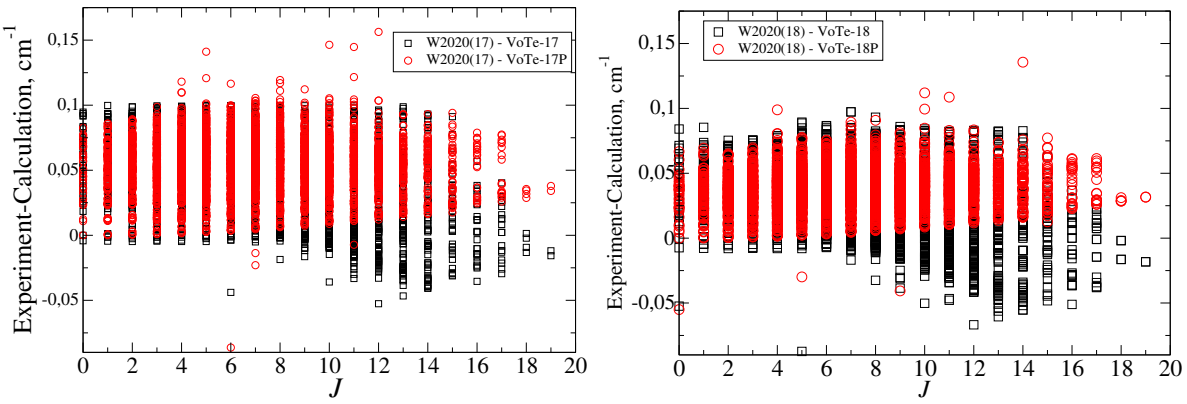

Figure (2) Illustration of the accuracy of the DVR3D calculations isotopologues of H_2O as obs.-calc. residuals between the 'experiment' (W2020) and theory (DVR3D) for two isotopologues for the set of 3426 states before and after substituting with the pseudo-experimental energies from Eq. (1), $H_2{}^{17}O$ (left display) and $H_2{}^{18}O$ (right display). W2020(17) and W2020(18) are the experimental energies, VoTe-17 and VoTe-18 are the DVR3D energies and VoTe-17P and VoTe-18P are DVR3D energies after the before the pseudo-experimental correction.

results obtained with the values from the W2020 compilation. For the set of 4127 levels of VoTe-17 (with error within 5 cm^{-1}), the obs.-calc. residuals between W2020 and corrected values of VoTe-17 produce an RMS error of 0.2646 cm^{-1}. This is very similar to the error indicators of VoTe-17 before applying the pseudo-experimental procedure, however the actual spread of the errors is improved by becoming more compact, see Fig. 2. The VoTe-18 energy term values corrected with the pseudo-experimental procedure give the RMS error of 0.6714 cm^{-1}.

The extensive analysis of the $H_2{}^{17}O$ and $H_2{}^{18}O$ calculated energies is to help estimate the errors of the DVR3D energies of $H_2{}^{15}O$, for which no data is available. One can argue that the accuracy of the DVR3D energies of $H_2{}^{15}O$ should be similar to that of the DVR3D energies of $H_2{}^{17}O$ as illustrated in Fig. 2. Moreover, the accuracy of the pseudo-experimental corrections in Eq. (1) applied to $H_2{}^{15}O$ should also be in line with that of $H_2{}^{17}O$, see Fig. 2, with the residuals appearing more compact after the pseudo-experimental corrections .

We decided to apply the pseudo-experimental correction only to our most confident set of 3426 levels to minimise chances of possible artefacts of this empirical procedure. For the set of 3426 levels the RMS error of the VoTe (16) energy levels from W2020 is 0.0266 cm^{-1}.

4. Isotopologue energy extrapolation

As an alternative to variational calculations, the energy levels of $H_2{}^{15}O$ can be estimated through extrapolation from the corresponding energies of $H_2{}^{16}O$, $H_2{}^{17}O$and $H_2{}^{18}O$ isotopologues as explored

by Bykov and Voronin [50]. According to this approach, an isotopic energy shift upon substitution of ^{16}O $\rightarrow$^{15}O is obtained using a quadratic expansion of the available experimental data for the $H_2{}^{16}O$ (16), $H_2{}^{17}O$(17) and $H_2{}^{18}O$ (18) in terms of the mass change μ in the form as given by (for details see[1, 50]).

$$E(H_2{}^{15}O)_{VR} = E(H_2{}^{16}O)_{VR} + \Delta E_{VR}, \tag{2}$$

where VR is the set of vibrational (V) and rotational (R) quantum numbers.

$$\Delta E_{VR} = \mu(15)\frac{\mu(18)^2({}^{17}E_{VR} - {}^{16}E_{VR}) + \mu(17)^2({}^{18}E_{VR} - {}^{16}E_{VR})}{\mu(17)\mu(18)(\mu(17) - \mu(18))} + \\ +\mu(15)^2\frac{\mu(18)({}^{17}E_{VR} - {}^{16}E_{VR}) + \mu(17)({}^{18}E_{VR} - {}^{16}E_{VR})}{\mu(17)\mu(18)(\mu(17) - \mu(18))}. \tag{3}$$

Here $\mu(N) = (m({}^{N}O) - m({}^{16}O))/m({}^{N}O)$ ($N = 15, 16, 17, 18$) is the relative change of the mass of the oxygen atom and ${}^{N}E_{VR}$ is the energy of the vibrational-rotational state VR of the isotopologue N, respectively. In our case, $\mu(15)$= -0.06610956879, $\mu(16)$=0.0, $\mu(17)$= 0.0590746134202 and $\mu(18)$= 0.1113521428953.

In fact, Eq. (2) can be considered as an application of the perturbation theory (PT), where the change in mass is a small parameter. We used Eq. (2) to generate PT energies of $H_2{}^{15}O$ for all 3426 vibrational-rotational states. Figure 3 compares these PT values to our DVR3D energies of $H_2{}^{15}O$. Apart from four clear outliers with differences of more than 12 cm^{-1}, (1 0 2) [14 4 11] 9618.1 cm^{-1}, (011) [15 6 9] 8856.1 cm^{-1}, (110) [14 4 11] 8011.9 cm^{-1} and (200) [12 4 8] 9359.6 cm^{-1}, the differences between the PT and DVR3D values are found to be within 5–10 cm^{-1}, which is at least an order of magnitude worse than the expected accuracy of the DVR3D values of $H_2{}^{15}O$. We therefore do not use the PT values for this study.

5. Line list

The line list for $H_2{}^{15}O$, which we call VoTe-15, designed for use at room temperature of a wide range of wavenumbers has been constructed. It contains 106 700 states and 149 665 544 (almost one hundred and fifty million) transitions in total. The $H_2{}^{15}O$ VoTe-15 line list is available from the ExoMol database www.exomol.com using the standard ExoMol format [51]. Extracts from the States `.states` and Transition `.trans` files are shown in Tables 2 and 3, respectively. The State file contains a list of ro-vibrational states of $H_2{}^{15}O$ with the state ID numbers, energy term values

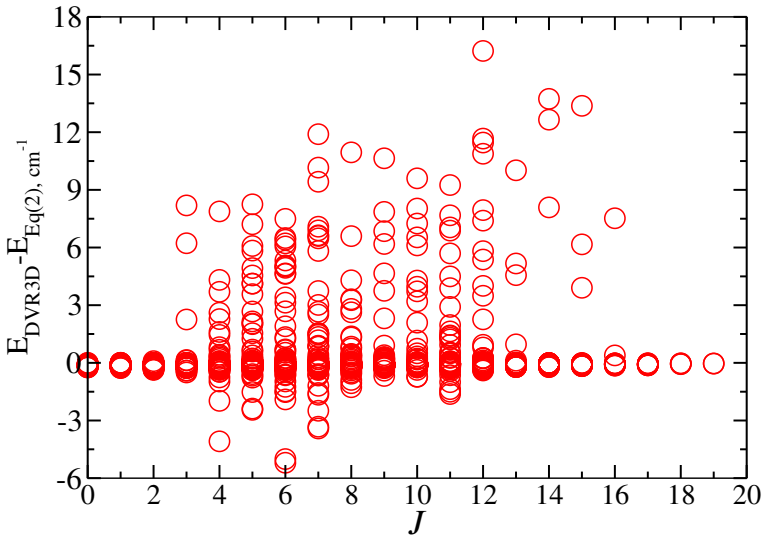

Figure (3) Comparison of energy levels of $H_2{}^{15}O$ calculated using DVR3D (E_{DVR3D}) and energy levels calculated using the isotopologue extrapolation technique in Eq. (2).

(in cm^{-1}), uncertainties (in cm^{-1}) and quantum numbers: the provision of which are discussed below. The exact quantum numbers are the total angular momentum J and the total symmetry $\Gamma = A_1, A_2, B_1, B_2$ in the Molecular Symmetry group C_{2v}(M). The total state degeneracy, g_i is given by (2J+1) times the nuclear spin factor, $g_{\rm ns}$. For $H_2{}^{15}O$ the nuclear spins $g_{\rm ns}$ are 2, 2, 6, and 6 for $\Gamma = A_1, A_2, B_1, B_2$, respectively, i.e. the nuclear degeneracy of the so-called ortho and para states relate as 6:2 (3:1 for $H_2{}^{16}O$). In addition, for some of the levels, approximate quantum numbers in the traditional rotation-vibrational identification v_1, v_2, v_3, K_a, K_c are also given; the provision of these is discussed below. Here v_1, v_2, v_3 are the normal mode vibrational quantum numbers, J is the (total) rotational angular momentum quantum number, K_a and K_c are the oblate and prolate rotational quantum numbers (projection of the angular momentum on the corresponding molecular axis a and c, respectively).

DVR3D only supplies rigorous quantum numbers which for H_2O correspond to J, parity and whether the state is ortho or para. To provide the approximate rotation and vibration quantum labels, namely v_1, v_2, v_3, K_a and K_c, we matched the $H_2{}^{15}O$ energies to the assigned states of the parent isotopologue $H_2{}^{16}O$ as provided in the VoTe line list, which was based on the calculations with the same PES [29, 30]. Following VoTe, here we also provide the parity of the K_c quantum number, which can be reconstructed from the (rigorous) values of J and the total symmetry Γ as shown in Table 12-7 of [52]. Here we adopt the ExoMol [53] standard and assign the value "NaN" to the undetermined values of the quantum numbers.

To improve the energy levels of $H_2{}^{15}O$, here we apply the pseudo-experimental corrections in Eq. (1) to the set of 3426 introduced above. These states are indicated with the label "IE" in contrast to all other, calculated values, labelled with "Ca".

The provision of uncertainties in the energy levels is now a formal part of the ExoMol data structure [53]. For the pseudo-experimental values, the uncertainties are estimated as the obs.-calc. residuals of the $H_2{}^{17}O$ isotopologue obtained as the difference between the W2020 and DVR3D energy values. When the rotational vibrational quantum numbers are available, the uncertainties can be estimated using the following approximate expression (in cm^{-1}), see, e.g. [54, 55]:

$$\text{unc} = \Delta\omega(v_1 + v_2 + v_3) + \Delta BJ(J+1), \tag{4}$$

for example $\Delta\omega$=0.2 cm^{-1} and ΔB=0.001 cm^{-1}. For this work, a slightly less conservative formula was used (in cm^{-1}):

$$\text{unc} = \Delta\xi\tilde{E} + \Delta BJ(J+1), \tag{5}$$

with $\Delta\xi$=1/35000 cm^{-1} and ΔB=0.0005 cm^{-1}. Formula (5) was obtained via correlation and auto-correlation methods [56] applied to the W2020 [46] data of the three isotopologues in conjunction with the method of Voronin [57].

It should be noted that Eq. (5) is more general than Eq. (4), especially if the vibrational quantum numbers are not available or not reliable. For $H_2{}^{16}O$, we can take the errors for 19225 levels from W2020(16), and calculate the errors using formula in (5).

3426 levels were replaced by the pseudo-experimental values. The maximum deviations of these changes do not exceed 0.1 cm^{-1}.

The $H_2{}^{15}O$ `.trans` files contain Einstein A coefficients (in s^{-1}) together with the upper and lower state ID numbers. The transitions are divided into twelve Transition files according the following spectroscopic ranges: 0–500, 500-1000, 1000-1500, 1500-2000, 2000-2500, 2500-3500, 3500-4500, 4500-5500, 5500-7000, 7000-9000, 9000-14000, 14000-25000 cm^{-1}.

6. Partition function

Using vibrational-rotational energy levels, the partition function of $H_2{}^{15}O$ was calculated for different temperatures up to 1200 K using

$$Q(T) = \sum_i g_i \exp\left(-\frac{E_i}{kT}\right). \tag{6}$$

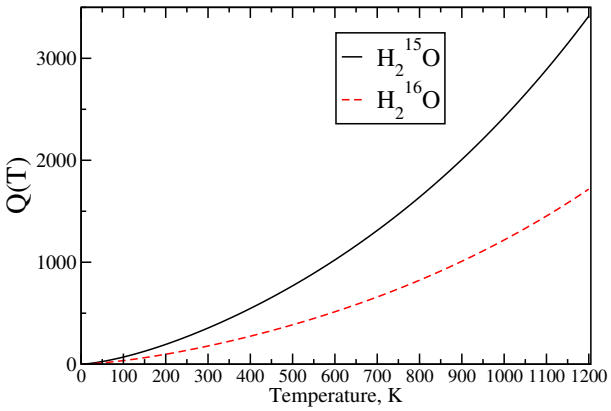

Figure (4) Partition function $Q(T)$ for $H_2{}^{16}O$ and $H_2{}^{15}O$ water for temperature range from 1 to 1200 K.

It is included into the ExoMol database and is also provided here as part of our supplementary material. The file format is quite simple, two columns with the temperature (K) and $Q(T)$.

Figure 4 shows a comparison of partition functions $Q(T)$ of the $H_2{}^{16}O$ and $H_2{}^{15}O$ species for the temperature range from 1 to 1200 K. The main difference is the nuclear spin factor, which is 2 times larger for $H_2{}^{15}O$. Besides, the partition function $Q(T)$ of $H_2{}^{16}O$ is significantly more complete, with the levels from [30] covering the rotational excitations up to $J = 50$.

In principle, with a set of levels up to 25000 cm^{-1} and up to $J = 30$, our partition function of $H_2{}^{15}O$ should be appropriate for up to 1000 K. Using it for higher temperatures can become increasingly incomplete. For more details see [58], [59]. See partition function table at Supplementary (partition-function-H215O.dat).

7. Spectral simulations

The line list produced was used to model atmospheric spectra of $H_2{}^{15}O$. The temperature step in atmospheric applications was taken, approximately, following the data in [60].

A room temperature $H_2{}^{15}O$ line list (296 K) was generated using the intensity threshold of $>10^{-30}$ cm/molecule for atmospheric applications. It contains 251 664 lines using the format similar to that of HITRAN2020 [61], see Table 4 and is provided as part of the supplementary material. The HITRAN database provides data for seven isotopologues of water using the following isotopologue codes: 11 ($H_2{}^{16}O$), 12 ($H_2{}^{18}O$), 13 ($H_2{}^{17}O$), 14($HD^{16}O$), 15($HD^{18}O$), 16($HD^{17}O$), 17 ($D_2^{18}O$). Here we adopted 18 as a code for $H_2{}^{15}O$ since this number is not yet taken in HITRAN. The line list consists of the isotopologue code (18) (Molecule number 1 + Isotopologue number 8), line positions, 296 K intensities (cm/molecule), Einstein coefficients (s^{-1}), air-broadened widths ($\gamma_{\rm air}$,

cm^{-1}/atm), self-broadened widths (γ_{self}, cm^{-1}/atm), temperature dependence component of air n_{air}, line shifts (set to 0.0 cm^{-1}) and ro-vibrational quantum number. The line broadening parameters were evaluated using the J and '$JJ-$dependency' methods [62]. For the temperature-dependence exponent n_{air} (unitless) we assumed the water vapor air-broadened half-widths from Table 7 of HITRAN2004 [63].

Table (1) Energy term values of $5\nu_2$ from W2020 for $H_2{}^{16}O$, $H_2{}^{17}O$, $H_2{}^{18}O$, all at cm^{-1}

$v_1v_2v_3$	JK_aK_c	$E_{H_2^{16}O}$	$E_{H_2^{17}O}$	$E_{H_2^{18}O}$	$E_{18}-E_{17}$	$E_{18}-E_{16}$
5 0 0	2 2 1	17021.8045	16997.1589	16975.4402	-21.71	-46.36
5 0 0	3 0 3	17024.2041	17000.6370	16979.7400	-20.89	-44.46
5 0 0	3 1 2	17059.2907	17035.5972	17014.7089	-20.88	-44.58
5 0 0	3 1 3	17029.0787	17005.3951	16984.4631	-20.93	-44.61
5 0 0	3 2 1	17094.6967	17070.0195	17048.2724	-21.74	-46.42
5 0 0	4 0 4	17102.8799	17079.1644	17058.1943	-20.97	-44.68
5 0 0	4 1 3	17154.2995	17130.3788	17109.2697	-21.10	-45.02
5 0 0	4 1 4	17105.2273	17081.3805	17060.2703	-21.11	-44.95
5 0 0	4 2 2	17192.2573	17167.5574	17145.6630	-21.89	-46.59
5 0 0	4 2 3	17176.6284	17151.5375	17129.4462	-22.09	-47.18
5 0 0	4 3 2	17255.8976	17229.2298	17205.7216	-23.50	-50.17
5 0 0	4 3 1	17257.2403	17230.6508	17248.4269	17.77	-8.81
5 0 0	5 0 5	17197.8448	17173.8339	17152.6107	-21.22	-45.23
5 0 0	5 1 4	17269.2800	17244.9289	17223.4671	-21.46	-45.81
5 0 0	5 1 5	17199.0210	17173.9360	17152.7043	-21.23	-46.31
5 0 0	5 2 3	17315.9505	17290.8244	17268.6750	-22.14	-47.27
5 0 0	5 2 4	17285.3295	17259.5306	17237.1224	-22.40	-48.20
5 0 0	5 3 2	17375.5385	17348.8711	17325.3789	-23.49	-50.15
5 0 0	5 3 3	17370.7139	17343.8599	17320.1298	-23.73	-50.58
5 0 0	6 0 6	17309.4283	17285.1060	17263.5701	-21.53	-45.85
5 0 0	6 1 5	17402.4115	17377.4830	17355.4532	-22.02	-46.95
5 0 0	6 1 6	17309.3737	17285.1049	17263.5485	-21.55	-45.82
5 0 0	6 2 4	17463.2753	17436.7237	17411.4610	-25.26	-51.81
5 0 0	7 1 6	17552.9104	17527.1509	17508.4680	-18.68	-44.44
5 0 0	7 1 7	17437.4399	17413.0614	17391.1775	-21.88	-46.26
5 0 0	7 3 4	17691.0999	17664.4216	17575.2641	-89.15	-115.83
5 0 0	8 2 7	17725.7266	17700.2148	17670.0464	-30.16	-55.68
5 0 0	8 3 6	17845.4255	17817.5993	17792.9552	-24.64	-52.47
5 0 0	10 2 9	18097.2548	18069.9088	18046.5019	-23.40	-50.75

Table (2) Extract from the `.states` file of the $H_2{}^{15}O$ line list.

i	$\tilde{E}$/cm^{-1}	g	J	δ/cm^{-1}	v_1	v_2	v_3	J	K_a	K_c	e/o	Γ_{tot}	$\tilde{E}_D$/cm^{-1}	Code
1	0.000000	2	0	0.000001	0	0	0	0	0	0	e	A1	0.000000	IE
2	1598.554996	2	0	0.000043	0	1	0	0	0	0	e	A1	1598.538460	IE
3	3158.978117	2	0	0.000036	0	2	0	0	0	0	e	A1	3158.973045	IE
4	3661.331777	2	0	0.000040	1	0	0	0	0	0	e	A1	3661.370183	IE
5	5243.021517	2	0	0.000316	0	3	0	0	0	0	e	A1	4677.467634	IE
6	5243.031283	2	0	0.000334	1	1	0	0	0	0	e	A1	5243.031283	IE
7	6147.780307	2	0	0.000640	0	4	0	0	0	0	e	A1	6147.774446	IE
8	6786.552879	2	0	0.000310	1	2	0	0	0	0	e	A1	6786.564864	IE
9	7210.728038	2	0	0.000907	2	0	0	0	0	0	e	A1	7210.730575	IE
...														
2088	22619.448202	10	2	0.648139	NaN	NaN	NaN	2	NaN	NaN	e	A1	22619.448202	Ca
2089	22621.337345	10	2	0.003716	7	0	0	2	0	2	e	A1	22621.316351	IE
2090	22628.228135	10	2	0.648517	NaN	NaN	NaN	2	NaN	NaN	e	A1	22628.228135	Ca
...														
2270	17049.225188	10	2	0.003776	4	0	1	2	2	1	o	A2	17049.226820	IE
2271	17183.145900	10	2	0.492886	NaN	NaN	NaN	2	NaN	1	o	A2	17183.145900	Ca
2272	17221.307627	10	2	0.493794	NaN	NaN	NaN	2	NaN	1	o	A2	17221.307627	Ca
2273	17348.315737	10	2	0.002550	2	2	2	2	1	1	o	A2	17348.325863	IE
2954	30472.486197	30	2	0.873642	NaN	NaN	NaN	2	NaN	1	o	B1	30472.486197	Ca
2955	30558.199397	30	2	0.876091	NaN	NaN	NaN	2	NaN	1	o	B1	30558.199397	Ca
2956	79.795500	30	2	0.000001	0	0	0	2	1	2	e	B2	79.795339	IE

i: state identifier;

$\tilde{E}$: state term value, DVR3D or pseudo-experimental;

g: state degeneracy;

J: state rotational quantum number;

δ: energy uncertainty;

$v_1 - v_3$: normal mode vibrational quantum numbers;

J: state rotational quantum number;

K_a and K_c: state oblate and prolate quantum numbers;

e/o even or odd - K_c: state oblate and prolate quantum numbers;

Γ_{tot}: total symmetry in C_{2v}(M).

$\tilde{E}_D$: state term value, DVR3D;

Code - Ca (Calculated by DVR3D) or IE - Isotopologue Extrapolation (Pseudo-experimental)

Table (3) Extract from a `.trans` file of the $H_2^{15}O$ line list.

f	i	A_{fi}
1967530	2157952	5.6990e-01
9281842	9684141	2.1589e-11
21248596	21941059	2.5861e-12
5252014	5149230	9.6459e-04
12481388	12623346	8.6482e-11
1781054	1841556	2.4679e-16

f: Upper state counting number;

i: Lower state counting number;

A_{fi}: Einstein-A coefficient (in s^{-1}).

Table (4) An extract from a recomputed VoTe-15 room temperature $H_2{}^{15}O$ absorption line list for atmospheric applications in HITRAN format.

C.	w.n. cm^{-1}	Intensity	A.coeff.	γ_{air}	γ_{self}	E_{low}	k_{Td}	shift	v_1' v_2' v_3'	J'	$K_a'K_c'$	v_1 v_2 v_3	J	K_aK_c
18	0.153696	0.944E-29	0.509E-10	0.0870	0.450	1927.454614	0.69	0.0	0 1 0	4	2 2	0 1 0	5	1 5
18	1.060925	0.935E-24	0.604E-08	0.0811	0.400	447.308191	0.69	0.0	NaNNaNNaN	6	NaNNaN	0 1 0	5	2 3
18	1.944495	0.914E-26	0.126E-06	0.0924	0.450	1824.052663	0.77	0.0	0 1 0	4	1 4	0 1 0	3	2 1
18	4.241993	0.202E-29	0.347E-06	0.0232	0.198	3630.296079	0.38	0.0	0 1 0	15	7 9	0 0 0	16	4 12
18	4.487160	0.178E-25	0.209E-05	0.0989	0.478	1743.715357	0.77	0.0	0 1 0	2	2 0	0 0 1	3	1 3
18	4.561485	0.303E-26	0.132E-05	0.0870	0.450	2132.427529	0.69	0.0	0 1 0	4	4 0	0 1 0	5	3 3
18	5.500705	0.646E-29	0.445E-05	0.0808	0.430	3875.009710	0.64	0.0	0 2 0	5	4 1	0 2 0	6	3 4
18	5.717382	0.686E-22	0.298E-05	0.0991	0.467	136.978676	0.78	0.0	0 0 0	3	1 3	0 0 0	2	2 0
18	5.742079	0.134E-27	0.870E-06	0.0284	0.207	2879.386079	0.36	0.0	0 0 0	14	4 10	0 0 0	15	3 13
18	5.870709	0.772E-29	0.442E-05	0.0925	0.467	3504.379365	0.73	0.0	0 2 0	3	3 1	0 2 0	4	2 2
18	6.099416	0.198E-27	0.124E-05	0.0284	0.207	3086.748618	0.36	0.0	0 0 0	14	6 9	0 0 0	15	3 12
18	6.163681	0.149E-29	0.367E-05	0.0991	0.467	3795.109362	0.78	0.0	1 0 0	3	1 3	1 0 0	2	2 0
18	6.675761	0.151E-28	0.167E-05	0.0232	0.198	3444.840632	0.38	0.0	0 0 0	15	6 10	0 0 0	16	3 13

C. - code - molecule number 1 + isotopologue number 8 = 18;

Transition wavenumber, cm^{-1};

Line Intensity at 100% abundance, cm/molecule ;

Einstein A-coefficient;

Air- broadened width, cm^{-1}/atm;

Self- broadened width, cm^{-1}/atm;

lower-state Energy, cm^{-1};

Temperature dependence (of air width), unitless;

Pressure shift, always zero in our case;

upper vibrational quanta, v_1', v_2', v_3';

upper local quanta, J', K_a', K_c';

lower vibrational quanta, v_1, v_2, v_3;

lower local quanta, J, K_a, K_c.

8. Possible laboratory and atmospheric applications

Previously [14], we focused on a possible detection of one absorption line of the $H_2{}^{15}O$ molecule. To do this, one us (Maria Makarova) studied atmospheric absorption in about 5,000 solar spectra with a special emphasis on days were there were thunderstorms. In the present work, with the help of our new $H_2{}^{15}O$ line list we attempt to identify more candidate $H_2{}^{15}O$ lines for possible future laboratory or atmospheric detection. Despite the difficulty associated with the minute concentration of $H_2{}^{15}O$ in the atmosphere, $H_2{}^{15}O$ should be detectable using IR-spectroscopy in the evaporation of radioactive water in a positron emission tomogography (PET) laboratory [14]. We therefore identify spectral intervals where the $H_2{}^{15}O$ lines are stronger and hence have a higher chance of being detected. To this end, transmission spectra of $H_2{}^{15}O$ and other water isotopologues were calculated using the line-by-line method [64] in the range from 0 to 10000 $cm^{-1}$with a spectral resolution of 0.01 cm^{-1}.

The intensity measured by a spectrometer is determined as

$$I(\tilde{\nu}) = \int\limits_{\Delta\tilde{\nu}} I_0(\tilde{\nu}')T(\tilde{\nu}')g(\tilde{\nu}' - \tilde{\nu})d\tilde{\nu}', \tag{7}$$

where $I_0(\tilde{\nu}')$ is the intensity of the source, $T(\tilde{\nu}')$ is the transmission function, $g(\tilde{\nu}')$ is the instrumental line shape function, $\tilde{\nu}$ is the wavenumber and $\Delta\tilde{\nu}$ is the spectral resolution.

The transmission function due to the absorption by atmospheric gases at the atmospheric vertical path from altitude z_1 to z_2 is calculated by

$$T(\tilde{\nu}) = \exp\left(-\int\limits_{z_1}^{z_2} \alpha_{\text{gas}}(\tilde{\nu}, p(z), T(z))dz\right), \tag{8}$$

where p is the atmospheric pressure, $T(z)$ is the temperature and $\alpha_{\text{gas}}(\tilde{\nu}, z)$ is the absorption coefficient at the altitude z. The absorption coefficient for the atmospheric gases is calculated using the line-by-line method, which takes into account all the absorption lines of the atmospheric gases in the spectral interval under consideration [64–66] as given by

$$\alpha_{\text{gas}}(\tilde{\nu}, z) = \sum_{i=1}^{N}\sum_{j=1}^{M} S_{ij}(p(z), T(z))f(\tilde{\nu}_{ij}^*, \tilde{\nu}, p(z), T(z))\rho_j(z), \tag{9}$$

where S_{ij} and $\tilde{\nu}_{ij}^*$ are the intensity and centre of the i^{th} line of the j^{th} gas, N is the number of spectral lines, M is the number of gases, $\rho_j(z)$ is the concentration of the j^{th} gas, and $f(\tilde{\nu}_{ij}^*, \tilde{\nu}, p(z), T(z))$ is

the function of the absorption line profile. A Voigt absorption line profile [67, 68] is generally used in atmospheric simulations.

The absorption line parameters, necessary for calculation of the absorption coefficient, are the line intensity, position of the line centre, lower-state energy of the transition, air-broadened half-width, self-broadened half-width, air pressure-induced line shift, and temperature-dependence exponent for air-broadened half-width. In the transmission simulation, our calculated $H_2{}^{15}O$ lines parameters were used. The information on line parameters of other atmospheric gases was taken from the HITRAN2020 spectroscopic database [61].

The spectral line intensities S_i in the HITRAN database and our calculations is given at a temperature of 296 K. To recalculate it to other temperatures, the following expression is applied [69]:

$$S_i(T) = S_i(T_0)\frac{Q(T_0)}{Q(T)}\frac{\exp(-E_i/kT)}{\exp(-E_i/kT_0)}\frac{[1-\exp(-hc\,\tilde{\nu}_i/kT)]}{[1-\exp(-hc\,\tilde{\nu}_i/kT_0)]} \tag{10}$$

where $Q(T)$ is the partition function which depends on the temperature T, h is Planck's constant, k is the Boltzmann constant, and c is the speed of light. We use our $Q(T)$ for $H_2{}^{15}O$ intensity recalculations; $Q(T)$ for other gases were taken from [70].

Initially, we simulated the transmission of the $H_2{}^{15}O$ for the laboratory conditions: a temperature of 300 K, atmospheric pressure of 1 atm, and a partial pressure of the water vapor of 0.26×10^5 ppm on a 100 m long path, see Fig. 5. Our transmission calculations suggest that $H_2{}^{15}O$ can be detected in radioactive water vapor at levels above 0.024% of $H_2{}^{16}O$. In the calculated spectrum shown here, the most promising intervals for detecting $H_2{}^{15}O$ are 1972–1974 cm^{-1}, and the spectral ranges around 3810, 3824.5 and 5276 cm^{-1}, see Figs.6. The spectral ranges around 3810 and 3824 cm^{-1} are suitable for the detection $H_2{}^{15}O$ in stated conditions, while the ranges near 1973 and 5276 cm^{-1} may be better used for detections with longer path lengths.

The atmospheric concentration of $H_2{}^{15}O$ increases during thunderstorms, which thus increases the possibility of observing a spectral fingerprint of $H_2{}^{15}O$ in tmeasured atmospheric spectra [14]. Here we estimate of the threshold $H_2{}^{15}O$ concentration which can be detected in the atmosphere by remote sensing with the use of spectroscopic methods. The measurement of the $H_2{}^{15}O$ content in the atmosphere at long path is difficult, even for the strongest lines, due to the overlap of $H_2{}^{15}O$ lines with other absorbing gases, some of which can be saturated (the atmospheric transmission at vertical path comes close to 0).

To estimate the possibility of detecting $H_2{}^{15}O$ lines in the atmosphere, the atmospheric trans-

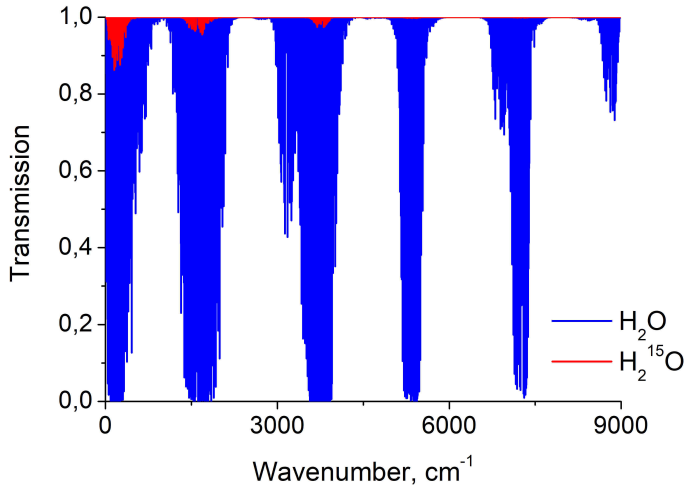

Figure (5) Transmission spectra of $H_2{}^{15}O$ and other H_2O isotopologues assuming an $H_2{}^{15}O/H_2O$ concentration ratio is 0.024%.

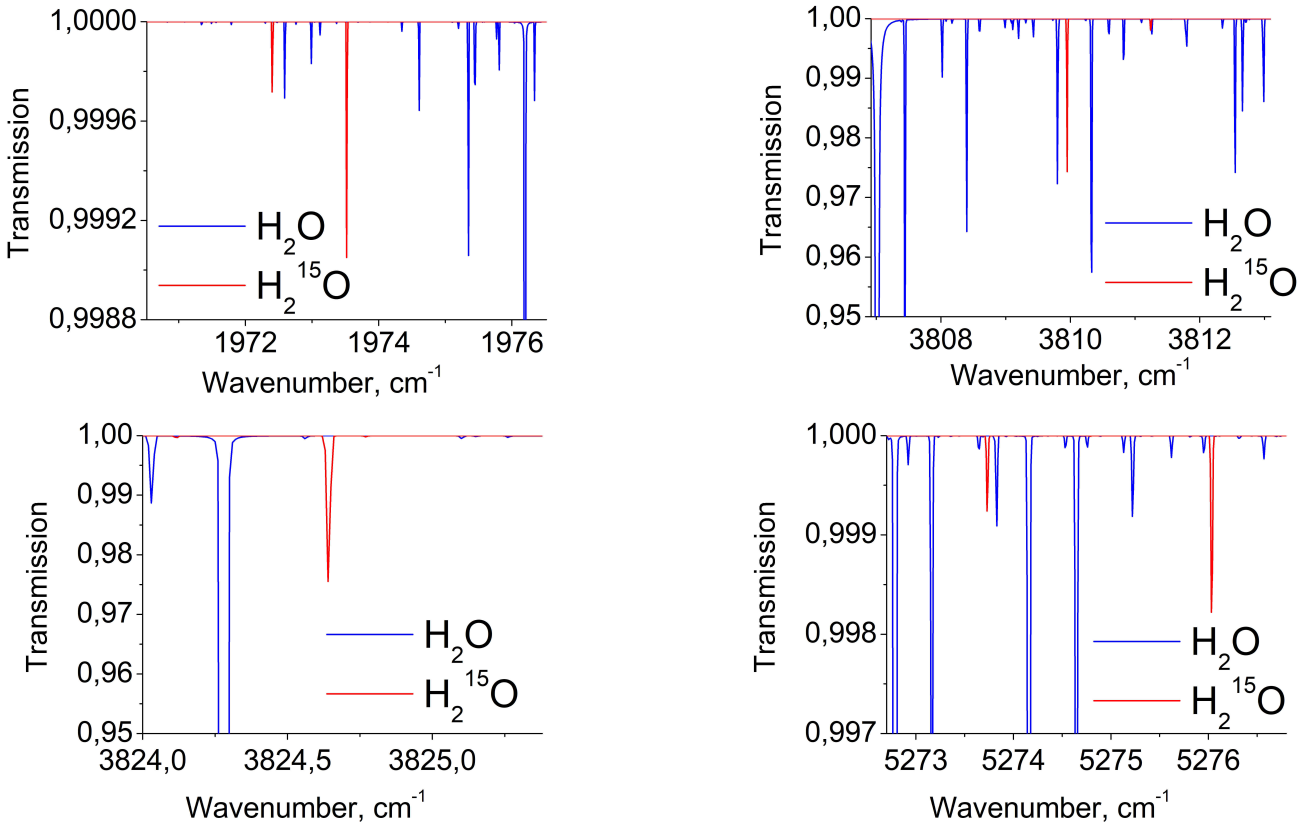

Figure (6) Prospective intervals for the detection of $H_2{}^{15}O$ in water vapor assuming an $H_2{}^{15}O/H_2O$ concentration ratio of 0.024%.

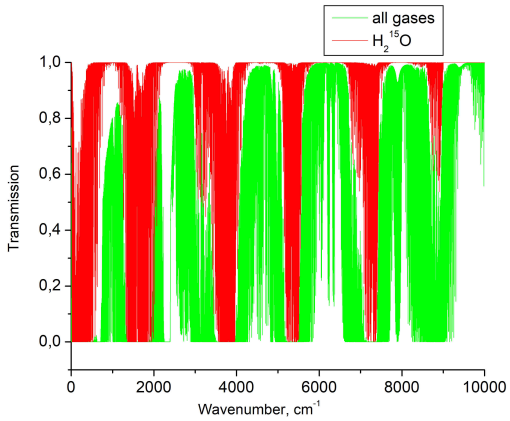

Figure (7) Atmospheric transmission of the main atmospheric gases (without $H_2{}^{15}O$) and $H_2{}^{15}O$ spectrum at the vertical path from 0 to 100 km for the mid latitude summer atmosphere with an $H_2{}^{15}O/H_2O$ concentrations ratio of 0.1%.

mission spectra were simulated at the vertical path from 0 to 100 km for a mid latitude summer meteorological model. The atmosphere was divided into 46 layers with constant values of temperature, pressure and concentration of gases. The atmospheric profiles were taken from the AFGL model [71] and were scaled to set the CO_2 content at 380 ppm, CH_4 at 1.8 ppm, O_3 at 300 DU (Dobson Unit). The column density of the water vapor (H_2O) was assumed at 3 g/cm^2. The atmospheric concentration of $H_2{}^{15}O$ was varied as percentage of the H_2O content. The atmospheric transmission was calculated using the line-by-line method [64] with a spectral resolution of 0.01 cm^{-1} using a Voigt line shape and boxcar apparatus function. The transmission simulations were carried out for different $H_2{}^{15}O$ atmospheric contencentrations to find the $H_2{}^{15}O$ detectability threshold. Our simulations suggest that a $H_2{}^{15}O/H_2O$ ratio above about 0.1% would allow the detection of the radioactive isotopologue $H_2{}^{15}O$ in the atmosphere. The atmospheric transmission spectrum of the main atmospheric gases and $H_2{}^{15}O$ spectrum with the concentration of 0.1% of the H_2O content, contained in AFGL profile, are presented in Fig. 7. Examples of perspective intervals for the $H_2{}^{15}O$ detection in the atmosphere are shown in Fig. 8.

9. Discussion

In the last couple of years, attempts have been made to obtain the IR spectrum of $H_2{}^{15}O$. It should be noted here that there are several problems with recording the spectrum of this isotopologue, including the following.

1. The costs of producing $H_2{}^{15}O$ (^{15}O and then $H_2{}^{15}O$) are very high, for example what we found

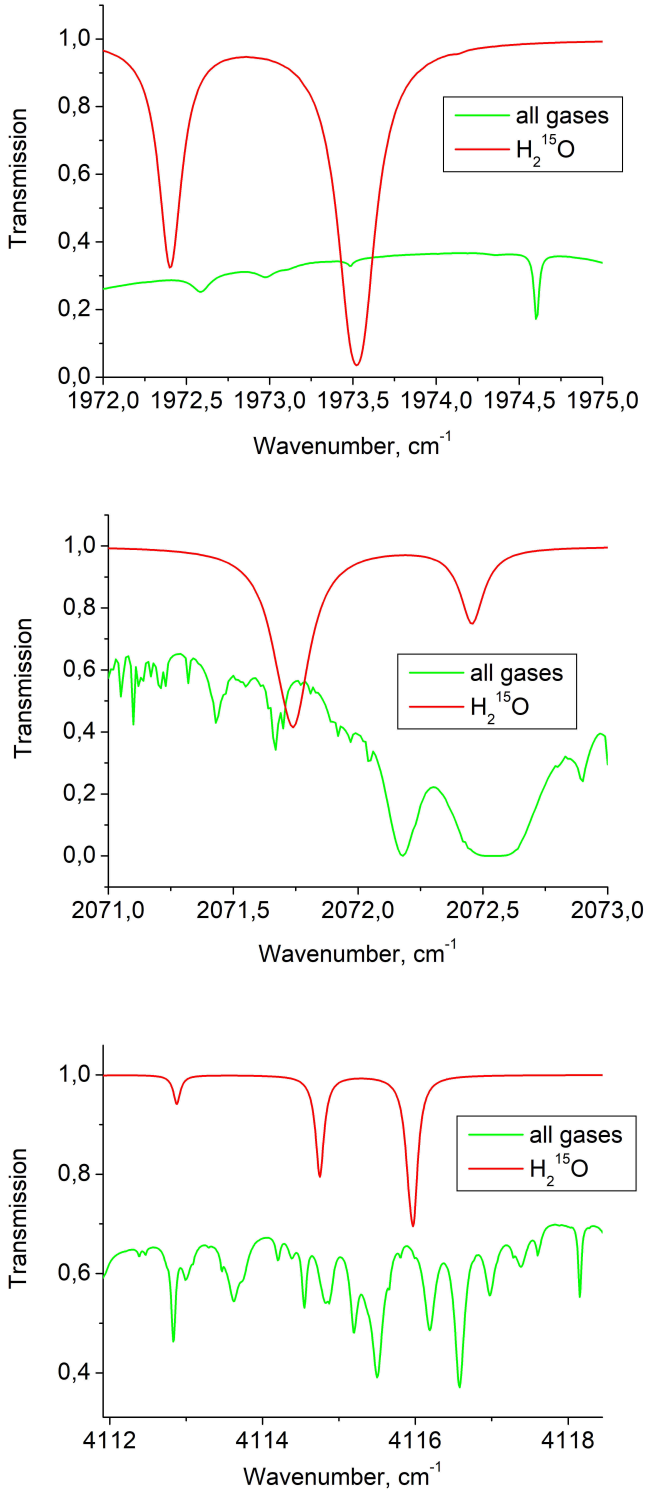

Figure (8) Promising spectral intervals for the detection of $H_2{}^{15}O$ in the Earth atmosphere

that preparing a small sample $H_2{}^{15}O$ using a cyclotron (at Tomsk Polytechnic University) was estimated at about US $100,000.

2. Naturally, the half-life $H_2{}^{15}O$ is about 2 minutes, which suggests that any measurements should take place quickly. Fourier spectroscopy is most likely not suitable for such laboratory measurements; Laser measurements are probably needed.
3. An experimental setup for recording the $H_2{}^{15}O$ spectrum should include a laser(s), an optical circuit and a receiving device. It is clear that this installation must be located in close proximity to the cyclotron, which can produce $H_2{}^{15}O$ with the cost of the installation components exceeding the cost of its production.

For atmospheric detection of $H_2{}^{15}O$, measurements in the tropics, or even at the equator, are the best. Thunderstorms provide especially promising mechanisms for production of $H_2{}^{15}O$, however the spectral measurements are complicated by the lack of the sunlight. Perhaps the best place to make atmospheric measurements to search for rare and short-lived molecules and radicals is the Maracaibo lagoon, and especially the mouth of the Catatumbo River, known as the "Maracaibo Lighthouse" [72]. However an expedition to a remote area of Venezuela, near the border with Colombia, would be challenging.

A more realistic scenario of detecting atmospheric $H_2{}^{15}O$ is to search the existing spectral archives of different atmospheric monitoring initiatives. The archive of the FTIR spectra of direct solar radiation contains data recorded using the high-resolution FTS (Fourier transform spectrometer) Bruker IFS 125HR installed at the St. Petersburg station (Faculty of Physics, St. Petersburg State University, a member of IRWG (Infrared Working Group) of NDACC (Network for the Detection of Atmospheric Composition Change) network, (https://ndacc.larc.nasa.gov/), https://www.ndaccdemo.org/stations/st-petersburg-russian-federation [73, 74]. This archive details dates and times of thunderstorm activity observed in the vicinity of St. Petersburg during 2011-2020. Previously[14], we analysed atmospheric spectra by combining of a large number ($\sim$4800) of measurements recorded under different atmospheric conditions over a period of 10 years, some including thunderstorms. This analysis hinted at the $H_2{}^{15}O$ absorption line at 1973.5 cm^{-1} as a possible candidate for detection of $H_2{}^{15}O$ absorption. This line could not be explained by any other gases present in the latest version of the HITRAN database [61]. In view of the fact that the individual spectra used in the compilation were recorded at different temperatures, pressures, and angles of the sun, it was not possible to fit spectral contours and determine the center of the

1973.5 cm^{-1} line accurately. The search for other $H_2{}^{15}O$ candidate lines in this compilation was difficult due to the peculiarities of the method used to record the atmospheric spectra and the use of filters to determine the concentrations of a number of gases in the NDACC network. One line is usually not enough for an unambiguous detection. In the present work, we suggest a number of spectroscopic ranges which can be used to search for the signature of $H_2{}^{15}O$ both in the Earth's atmospheric and also in laboratory experiments.

The archive of spectra that was used in work [14] has a number of limitations, such as the operating range of the Fourier spectrometer, filters, etc. The calculated spectrum has no such limitations. Our current line list can provide spectra for fairly high temperatures, up to 1000 K, which is important for plasma and lightning. It is more complete and perhaps more accurate.

In total, 8 promising transitions were selected, which are collected in Table 5. Of the 16 levels that make up these 8 transitions, 15 have been replaced by the pseudo-experimental values.

The six lines illustrated in Fig. 6 were selected as most promising candidates detection laboratory experiments. Three lines, illustrated in Figs.8, were identified as most promising candidates for atmospheric detection experiments. Line 1973.5 cm^{-1} is the most suitable candidate for detection both in the laboratory and in the atmosphere.

It is clear that on the one hand there is a difficulty in obtaining the $H_2{}^{15}O$ water in nature or in the lab. On the other hand, there are difficulties with controlling the concentration, which will decrease very quickly. Therefore, it is logical to expect rather qualitative than quantitative characterisation of the $H_2{}^{15}O$ spectra, at least at the first stage.

The only line that has been analyzed to date deserves a little more discussion. After carrying out certain clarifications, the center of the line 1973.521 cm^{-1} from [14] was optimistically refined as 1973.52015 ± 0.00047 cm^{-1}. It should be noted that both the center itself and the errors in its definition must be treated with caution.

According to our DVR3D calculations, a closest strong $H_2{}^{15}O$ line is 1973.5228 cm^{-1}, assigned (010) [7 5 3] - (000) [6 4 2] . Using the PT formulas in Eqs. (3) and (2), in conjunction with the W2020 energy values of $H_2{}^{16}O$, $H_2{}^{17}O$ and $H_2{}^{18}O$, this line is obtained as 1973.593906 cm^{-1}, which differs from the experimental line by -0.073756 cm^{-1}. If, however, we use the pseudo-experimental procedure in Eq. (1) from [28], we obtain 1973.54461 cm^{-1}, which is only -0.024459 cm^{-1} away from the 'experimental' value. Comparison with the DVR3D calculation gives the best agreement of -0.002694 cm^{-1}. This is still not sufficient to claim a detection with only one coinciding line

between theory and experiment. Only more laboratory measurements can give a definitive answer.

The main limitation of this study is the absence of experimental data on $H_2{}^{15}O$ due to the rather expensive samples of oxygen-15 and the associated recording of the spectrum as the apparatus must be resistant to radioactive radiation. Therefore accurate predictions are especially important with the promising candidate at 1973 cm^{-1}.

A detection of water-15 in laboratory or natural conditions would offer a number of important applications. For example, in medicine, water-15 observations could provide better control of the radiochemical drug treatment which is administered to patients during PET tomography. In plasma science, water-15 could help with separation of radioactive substances as sources of radiation in slow discharges. For atmospheric applications, the spectrum of water-15 could help understand the physics and chemistry of lightning in the Earth atmosphere.

10. Conclusions

As a result of this work, we can offer the following conclusions. An empirical ExoMol line list for the $H_2{}^{15}O$ isotopologue is presented. It is computed using the spectroscopic model optimised for $H_2{}^{16}O$ and covers all transitions up to J=30 and should be valid for temperatures up to 1200 K. The quality of the line list was systematically improved through an isotopoic extrapolation of experimental energies of $H_2{}^{16}O$, $H_2{}^{17}O$ and $H_2{}^{18}O$. Until any spectroscopic measurements of $H_2{}^{15}O$, this accurate theoretical line list is only data available for future detection of $H_2{}^{15}O$.

Several promising lines for the detection of $H_2{}^{15}O$ in laboratory or atmospheric conditions are presented. Of these, only the transition 1973.5 cm^{-1} was possible to match with a line from the compilation of atmospheric experiments in [14].

The IR spectrum of $H_2{}^{15}O$ offers scientists a new tool for medicine for medical(quality control of radiochemical pharmaceuticals for PET tomography), physical (plasma physics, nuclear physics) and astrophysical applications (as a new search object). Controlling the concentration of $H_2{}^{15}O$ when injecting, understanding the chemistry of plasma, understanding what happens in the atmosphere after thunder and lightning, everything is important. A qualitatively calculated spectrum of $H_2{}^{15}O$ can be considered a zero step for solving the assigned problems. Obtaining solar spectra, and especially archives containing numerous, long-term measurements, is also a separate difficulty, since it is of undoubted value for the measuring side.

Table (5) . A selection of promising theoretical $H_2{}^{15}O$ lines at T=300 K and $P = 1$ atm with the corresponding lower state energies and quantum number for detection in atmospheric conditions computed using the new $H_2{}^{15}O$ line list presented here. The lower vibrational quantum numbers are equal to zero, for all transitions in this table and are not presented. (v_1'' =v_2''= v_3''=0)

DVR3D	Int	$\tilde{E}_{\rm low}$	v_1' v_2' v_3'	$J'K_a'K_c'$	$J''K_a''K_c''$	DVR−Eq. (2)	DVR−Eq. (1)
1972.403564	0.25E-20	761.083642	0 1 0	7 5 3	6 4 2	-0.073282	0.021798
1973.522827	0.75E-20	760.082267	0 1 0	7 5 2	6 4 3	-0.073756	0.021765
2071.740967	0.15E-20	1052.047083	0 1 0	7 7 0	6 6 1	-0.118860	0.062323
3809.949463	0.24E-18	23.817501	0 0 1	2 0 2	1 0 1	-0.050513	-0.006071
3824.770264	0.18E-20	70.185887	0 0 1	2 2 1	2 0 2	-0.057397	-0.001669
4115.917480	0.28E-21	510.637887	0 0 1	6 5 1	5 3 2	-0.072510	-0.001774
5273.732422	0.93E-20	212.958918	0 1 1	2 2 0	3 2 1	-0.095154	0.000975
5276.033691	0.24E-19	137.008484	0 1 1	2 0 2	3 0 3	-0.088700	-0.001815

11. Data availability

The full line list is provided via the ExoMol website www.exomol.com.

File `partition-function-H215O.dat` containing only 2 columns, can be found in the supplementary materials. In the first column, the temperature in K, from 1 to 1200 K, in the second column, the value of the partition function for a given temperature.

File H215O-spectra-296K-E30.dat as at table (4) can be found in the supplementary materials.

At https://ftp.iao.ru/pub/VTT/H215O/ALL/ there are 15 files: 12 files containing transitions divided into ranges (format is described in the table 3); one file with the energy levels and identification; one file for atmospheric applications in a format like HITRAN database and one file as an archive for easy download.

At https://ftp.iao.ru/pub/VTT/H215O/SpectraH215O/ReadMe-H215O-J10, the explanation and notation for the file with atmospheric application are provided.

Author Statement

Boris A. Voronin: Term, Validation, Investigation, Writing - Original Draft; **Jonathan Tennyson**: Supervision, Conceptualization, Resources, Writing - Review & Editing, Methodolog; **Sergey N. Yurchenko**: Methodology, Validation, Data Curation, Writing - Review & Editing;

Tatyana Yu. Chesnokova: Investigation, Data Curation, Writing - Review & Editing; **Aleksei V. Chentsov**: Formal analysis, Visualization; **Maria V. Makarova**: Data Curation, Resources; **Aleksandr D. Bykov**: Conceptualization, Validation. **Svetlana S. Voronina**: Formal analysis; **Flávio C. Cruz**: Supervision, Funding acquisition.

Declaration of Competing Interest

None of the authors declare a conflict of interest.

Acknowledgement

The work was partially supported by the MSHE RF (V.E. Zuev IAO SB RAS) and NERC grant NE/F01967X/1. Boris Voronin is grateful for the financial support of the grant - FAPESP (2022/08772-1).

References

[1] Voronin, B.A., Bykov, A.D.. Calculation of vibrational levels of $H_2{}^XO$ (where X=11,...,26). Proceedings of SPIE 2021;11916:1191605. doi:10.1117/12.2603166.

[2] Gurov, Y.B., Aleshkin, D.V., Behr, M.N., Lapushkin, S.V., Morokhov, P.V., Pechkurov, V.A., et al. Spectroscopy of superheavy hydrogen isotopes in stopped-pion absorption by nuclei. Physics of Atomic Nuclei 2005;68(3):491 – 497. doi:10.1134/1.1891200.

[3] Korsheninnikov, A.A., Nikolskii, E.Y., Kuzmin, E.A., Ozawa, A., Morimoto, K., Tokanai, F., et al. Experimental Evidence for the Existence of ^{7}H and for a Specific Structure of ^{8}He. Phys Rev Lett 2003;90:082501. doi:10.1103/PhysRevLett.90.082501.

[4] Webb, T., Wang, S., Brown, K.W., Charity, R.J., Elson, J., Barney, J., et al. First Observation of Unbound ^{11}O, the Mirror of the Halo Nucleus ^{11}Li. Phys Rev Lett 2018;122:122501. doi:10.1103/PhysRevLett.122.122501.

[5] Kondo, Y., Achouri, N.L., Al Falou, H., Atar, L., Aumann, T., Baba, H., et al. First observation of 28O. Nature 2023;620:965–970. doi:10.1038/s41586-023-06352-6.

[6] Down, M.J., Tennyson, J., Hara, M., Hatano, Y., Kobayashi, K.. Analysis of a tritium enhanced water spectrum between 7200 – 7245 cm^{-1} using new variational calculations. J Mol Spectrosc 2013;289:35–40. doi:10.1016/j.jqsrt.2013.05.027.

[7] Mikhailenko, S.N., Babikov, Y.L., Golovko, V.F.. Information-calculating system spectroscopy of atmospheric gases. the structure and main functions. Atmospheric Ocean Opt 2005;18:685–695. doi:10.1161/01.STR.29.7.1281.

[8] West, J.B., Dollery, C.T.. Absorption of inhaled radioactive water vapour. Nature 1961;189:588–588. doi:doi:10.1038/189588a0.

[9] Welch, M.J., Lifton, J.F., Ter-Pogossian, M.M.. Preparation of millicurie quantities of oxygen-15 labeled water. J Label Compd Radiopharm 1969;5:168–172. doi:10.1002/jlcr.2590050210.

[10] Eichling, J.O., Raichle, M.E., Grubb, R.L., Larson, K.B., Ter-Pogossian, M.M.. In vivo determination of cerebral blood volume with radioactive oxygen-15 in the monkey. Circ Res 1975;37:707–714. doi:10.1161/01.RES.37.6.707.

[11] Nariai, T., Senda, M., Ishii, K., Wakabayashi, S., Yokota, T., Toyama, H., et al. Posthyperventilatory steal response in chronic cerebral hemodynamic stress. Stroke 1998;29:1281–1292. doi:10.1161/01.STR.29.7.1281.

[12] Chareonthaitawee, P., Christenson, S.D., Anderson, J.L., Kemp, B.J., Hodge, D.O., Ritman, E.L., et al. Reproducibility of Measurements of Regional Myocardial Blood Flow in a Model of Coronary Artery Disease: Comparison of $H_2^{15}O$ and $^{13}NH_3$ PET Techniques . Journal of Nuclear Medicine 2006;47(7):1193–1201.

[13] Karoui, C., Strelnikov, K., Payoux, P., Salabert, A.S., James, C.J., Deguine, O., et al. Auditory cortical plasticity after cochlear implantation in asymmetric hearing loss is related to spatial hearing: a PET $H_2^{15}O$ study. Cerebral Cortex 2022;33:2229–2244. doi:10.1093/cercor/bhac204.

[14] A., B., Makarova, M.V., Poberovskii, A.V., Bykov, A.D., Dudnikiva, E.A., Tennyson, J.. The absorption spectrum of short-lived isotopic variant of water, $H_2^{15}O$: Tentative detection at the Earth's atmosphere. J Quant Spectrosc Radiat Transf 2021;276:107929. doi:10.1016/j.jqsrt.2021.107929.

[15] Babich, L.P.. Thunderous neutrons. Phys Usp 2019;62:976–999. doi:10.3367/UFNe.2018.12.038501.

[16] Dwyer, J.R., Smith, D.M., Hazelton, B.J., Grefenstette, B.W., Kelley, N.A., Lowell, A.W., et al. Positron clouds within thunderstorms. J Plasma Physics 2015;81:475810405. doi:10.1017/S0022377815000549.

[17] Kobayashi, M., Kiyono, Y., Maruyama, R., Mori, T., Kawai, K., Okazawa, H.. Development of an $H_2^{15}O$ steady-state method combining a bolus and slow increasing injection with a multiprogramming syringe pump. J Cereb Blood Flow Metab 2011;31:527–534. doi:10.1038/jcbfm.2010.122.

[18] Powers, W.J., Stabin, M., Howse, D., Eichung, J.O., Herscovitch, P.. Radiation Absorbed Dose Estimatesfor Oxygen-15 Radiopharmaceuticals ($H_2^{15}O$, $C^{15}O$, $O^{15}O$) in Newborn Infants. J Nucl Med 1988;29:1961–1970.

[19] Chernov, V.I., Goncharova, N.M., Goldberg, V.E., Dudnikova, E.A., Zelchan, R.V., Medvedeva, A.A., et al. The value of PET/CT in the diagnosis, stading and monitoring of colorectal cancer. Siberian J Oncol 2019;18:67–77. doi:10.21294/1814-4861-2019-18-4-67-77.

[20] Saha, G.B., MacIntyre, W.J., Go, R.T.. Radiopharmaceuticals for brain imaging. Semin Nucl Med 1994;24:324–349. doi:10.1016/s0001-2998(05)80022-4.

[21] Dowsett, D.. Radiological Sciences Dictionary: Keywords, Names and Definitions. 1 ed.; London: Hodder Arnold; 2009. doi:10.1201/b:13300.

[22] Bubukina, I.I., Polyansky, O.L., Zobov, N.F., Yurchenko, S.N.. Optimized semiempirical potential energy surface for $H_2{}^{16}O$ up to 26000 cm^{-1}. Opt Spectrosc 2011;110:160–166. doi:10.1134/S0030400X11020032.

[23] Lodi, L., Tennyson, J., Polyansky, O.L.. A global, high accuracy ab initio dipole moment surface for the electronic ground state of the water molecule. J Chem Phys 2011;135:034113. doi:10.1063/1.3604934.

[24] Tennyson, J., Kostin, M.A., Barletta, P., Harris, G.J., Polyansky, O.L., Ramanlal, J., et al. DVR3D: a program suite for the calculation of rotation-vibration spectra of triatomic molecules. Comput Phys Commun 2004;163:85–116.

[25] Voronin, B.A., Tennyson, J., Tolchenov, R.N., Lugovskoy, A.A., Yurchenko, S.N.. A high accuracy computed line list for the HDO molecule. Mon Not R Astron Soc 2010;402:492–496.

[26] Polyansky, O.L., Kyuberis, A.A., Zobov, N.F., Tennyson, J., Yurchenko, S.N., Lodi, L.. ExoMol molecular line lists XXX: a complete high-accuracy line list for water. Mon Not R Astron Soc 2018;480:2597–2608. doi:10.1093/mnras/sty1877.

[27] Conway, E.K., Gordon, I.E., Kyuberis, A.A., Polyansky, O.L., Tennyson, J., Zobov, N.F.. Accurate line lists for $H_2{}^{16}O$, $H_2{}^{18}O$ and $H_2{}^{17}O$ with extensive comparisons to theoretical and experimental sources including the HITRAN2016 database. J Quant Spectrosc Radiat Transf 2020;241:106711. doi:10.1016/j.jqsrt.2019.106711.

[28] Polyansky, O.L., Kyuberis, A.A., Lodi, L., Tennyson, J., Ovsyannikov, R.I., Zobov, N.. ExoMol molecular line lists XIX: high accuracy computed line lists for $H_2{}^{17}O$ and $H_2{}^{18}O$. Mon Not R Astron Soc 2017;466:1363–1371. doi:10.1093/mnras/stw3125.

[29] Voronin, B.A., Tennyson, J., Lodi, L.. The VoTe room temperature $H_2{}^{16}O$ line list up to 25000 cm^{-1}. In: 24th International Symposium on Atmospheric and Ocean Optics: Atmospheric Physics; vol. 10833. 2018, p. 10833H. doi:10.1117/12.2504466.

[30] Voronin, B.A., Tennyson, J., Lodi, L., Kozodoev, A.. The VoTe room temperature $H_2{}^{16}O$ line list up to 25000 cm^{-1}. Opt Spectrosc 2019;117:967–973. doi:10.1134/S0030400X19120397.

[31] Bykov, A.D., Makushkin, Y.S., Ulenikov, O.N.. On isotope effects in polyatomic molecules: Some comments on the method. Journal of Molecular Spectroscopy 1981;85:462–479. doi:10.1016/0022-2852(81)90217-4.

[32] Bykov, A.D., Makushkin, Y.S., Ulenikov, O.N.. On the displacements of centers of vibration-rotation bands under isotope substitution in polyatomic molecules. Journal of Molecular Spectroscopy 1982;93:46–54. doi:10.1016/0022-2852(82)90273-9.

[33] Fowler, P.W.. Perturbation calculation of isotope shifts in molecular properties. Molecular Physics 1983;48:153–160. doi:10.1080/00268978300100101.

[34] Schwenke, D.W.. First principles prediction of isotopic shifts in H2O. The Journal of Chemical Physics 2003;118:6898–6904.

URL: https://doi.org/10.1063/1.1561053. doi:10.1063/1.1561053. arXiv:https://pubs.aip.org/aip/jcp/article-pdf/118/15/6898/12244161/6898_1_online.pdf.

[35] Chesnokov, E.N., Gorelik, S.R., Gritsan, N.P.. Calculations of the isotopic shifts of fundamental frequencies for dihaloid silanes. Vibrational Spectroscopy 2003;32:241–248. doi:10.1016/S0924-2031(03)00065-1.

[36] Khriachtchev, L., Lundell, J., Pettersson, M., Tanskanen, H., Räsänen, M.. Anomalous isotopic effect on vibrational properties of HXeOH. The Journal of Chemical Physics 2002;116:4758–4761. doi:10.1063/1.1459703.

[37] Loëte, M., Richard, C., Boudon, V.. Isotopic relations for tetrahedral and octahedral molecules. Journal of Molecular Structure 2020;1206:127729. URL: https://www.sciencedirect.com/science/article/pii/S0022286020300533. doi:10.1016/j.molstruc.2020.127729.

[38] Bykov, A.D., Voronin, B.A., Dudaryonok, A.S., Polovtseva, E.R.. Shift of vibrational bands upon isotope substitution in molecules. Atmos Oceanic Optics 2021;34(4):237–244. doi:DOI:10.15372/AOO20210401.

[39] Huang, X., Schwenke, D.W., Lee, T.J.. Empirical infrared line lists for five SO2 isotopologues: 32/33/34/36S16O2 and 32S18O2. Journal of Molecular Spectroscopy 2015;311:19–24. doi:10.1016/j.jms.2015.01.010; theory and Spectroscopy.

[40] Polyansky, O.L., Ovsyannikov, R.I., Kyuberis, A.A., Lodi, L., Tennyson, J., Zobov, N.F.. Calculation of rotation-vibration energy levels of the water molecule with near-experimental accuracy based on an ab initio potential energy surface. J Phys Chem A 2013;117:9633–9643. doi:10.1021/jp312343z.

[41] Viglaska-Aflalo, D., Rey, M., Nikitin, A., Delahaye, T.. A global view of isotopic effects on ro-vibrational spectra of six-atomic molecules: a case study of eleven ethylene species. Phys Chem Chem Phys 2020;22:3204–3216. doi:10.1039/C9CP06383H.

[42] Partridge, H., Schwenke, D.W.. The determination of an accurate isotope dependent potential energy surface for water from extensive ab initio calculations and experimental data. J Chem Phys 1997;106:4618–4639. doi:10.1063/1.473987.

[43] Wang, M., Huang, W.J., Kondev, F.G., Audi, G., Naimi, S.. The AME 2020 atomic mass evaluation (II). Tables, graphs and references. Chin Phys C 2021;45:030003. doi:10.1088/1674-1137/abddaf.

[44] Császár, A.G., Czako, G., Furtenbacher, T., Tennyson, J., Szalay, V., Shirin, S.V., et al. On equilibrium structures of the water molecule. J Chem Phys 2005;122:214305.

[45] Hobson, S.L., Valeev, E.F., Csaszar, A.G., Stanton, J.F.. Is the adiabatic approximation sufficient to account for the post-born-oppenheimer effects on molecular electric dipole moments? Mol Phys 2009;107:1153–1159. doi:10.1080/00268970902780262.

[46] Furtenbacher, T., Tóbiás, R., Tennyson, J., Polyansky, O.L., Császár, A.G.. W2020: A Database of Validated Rovibrational Experimental Transitions and Empirical Energy Levels of $H_2{}^{16}O$. J Phys Chem Ref Data 2020;49:033101. doi:10.1063/5.0008253.

[47] Zobov, N.F., Shirin, S.V., Polyansky, O.L., Tennyson, J., Coheur, P.F., Bernath, P.F., et al. Monodromy in the water molecules. Chem Phys Lett 2005;414:193–197.

[48] Bykov, A., Naumenko, O., Sinitsa, L., Voronin, B., Flaud, J.M., Camy-Peyret, C., et al. High-order resonances in the water molecule. Journal of Molecular Spectroscopy 2001;205:1–8. doi:10.1006/jmsp.2000.8231.

[49] McKemmish, L.K., Syme, A.M., Bowesman, C.A., Kefela, K., Yurchenko, S.N., Tennyson, J.. A hybrid approach to generating diatomic line lists for high resolution studies of exoplanets and other hot astronomical objects: Updates to ExoMol MgO, VO and TiO line lists. RAS Tech Instr 2024;(in preparation).

[50] Bykov, A.D., Voronin, B.A.. Shift of vibrational energy levels of molecules under isotoposubstitution. Isotopic series. Atmos Oceanic Optics 2023;36:339–345. doi:10.15372/AOO20230501.

[51] Tennyson, J., Hill, C., Yurchenko, S.N.. Data structures for ExoMol: Molecular line lists for exoplanet and other atmospheres. In: 6^{th} international conference on atomic and molecular data and their applications ICAMDATA-2012; vol. 1545 of *AIP Conference Proceedings*. AIP, New York; 2013, p. 186–195. doi:10.1063/1.4815853.

[52] Bunker, P.R., Jensen, P.. Molecular symmetry and spectroscopy. 2 ed.; Ottawa: NRC Research Press; 1998. doi:10.1142/p371.

[53] Tennyson, J., Yurchenko, S.N., Al-Refaie, A.F., Clark, V.H.J., Chubb, K.L., Conway, E.K., et al. The 2020 release of the ExoMol database: Molecular line lists for exoplanet and other hot atmospheres. J Quant Spectrosc Radiat Transf 2020;255:107228. doi:10.1016/j.jqsrt.2020.107228.

[54] Tarczay, G., Császár, A.G., Polyansky, O.L., Tennyson, J.. Ab initio rovibrational spectroscopy of hydrogen sulphide. J Chem Phys 2001;115:1229–1242.

[55] Mellor, T., Owens, A., Yurchenko, S.N., Tennyson, J.. ExoMol line lists – LI. Rvibronic molecular line list for thioformaldehyde (H_2CS). Mon Not R Astron Soc 2022;520:1997–2008. doi:10.1093/mnras/stad111.

[56] Box, G.E.P., Jenkins, G.M., Reinsel, G.C.. Time Series Analysis: Forecasting and Control. Wiley Series in Probability and Statistics; Wiley; 2013. ISBN 9781118619063. URL: https://books.google.com.br/books?id=jyrCqMBW_owC.

[57] Voronin, B.A.. Method of estimation of self-broadening parameters of spectroscopic lines on the example of the $^{32}S^{16}O_2$ molecule. Atmospheric Ocean Opt 2020;33:849–853. doi:10.15372/AOO20201104.

[58] Harris, G.J., Viti, S., Mussa, H.Y., Tennyson, J.. Calculated high temperature partition function and related thermodynamic data for $H_2{}^{16}O$. J Chem Phys 1998;109:7197–7204.

[59] Vidler, M., Tennyson, J.. Accurate partition function and thermodynamic data for water. J Chem Phys 2000;113:9766–9771.

[60] Fischer, J., Gamache, R., Goldman, A., Rothman, L., Perrin, A.. Total internal partition sums for molecular species in the 2000 edition of the hitran database. J Quant Spectrosc Radiat Transf 2003;82:401–412. doi:10.1016/S0022-4073(03)00166-3; the HITRAN Molecular Spectroscopic Database: Edition of 2000 Including Updates of 2001.

[61] Gordon, I.E., Rothman, L.S., Hargreaves, R.J., Hashemi, R., Karlovets, E.V., Skinner, F.M., et al. The HITRAN2020 molecular spectroscopic database. J Quant Spectrosc Radiat Transf 2022;277:107949. doi:10.1016/j.jqsrt.2021.107949.

[62] Voronin, B.A., Lavrentieva, N.N., Mishina, T.P., Y.Chesnokova, T., Barber, M.J., Tennyson, J.. Estimate of the $J'J''$ dependence of water vapor line broadening parameters. J Quant Spectrosc Radiat Transf 2010;111:2308–2314.

[63] Rothman, L.S., Jacquemart, D., Barbe, A., Benner, D.C., Birk, M., Brown, L.R., et al. The *HITRAN* 2004 molecular spectroscopic database. J Quant Spectrosc Radiat Transf 2005;96:139–204. doi:10.1016/j.jqsrt.2004.10.008.

[64] Mitsel, A.A., Ptashnik, I.V., Firsov, K.M., Fomin, B.A.. Efficient technique for line-by-line calculating the transmittance of the absorbing atmosphere. Atmospheric Ocean Opt 1995;8:847–850.

[65] Kuntz, M., Höpfner, M.. Efficient line-by-line calculation of absorption coefficients. J Quant Spectrosc Radiat Transf 1999;63(1):97–114. URL: https://www.sciencedirect.com/science/article/pii/S002240739800140X. doi:https://doi.org/10.1016/S0022-4073(98)00140-X.

[66] Tan, X.. An ultrafast line-by-line algorithm for calculating spectral transmittance and radiance. J Quant Spectrosc Radiat Transf 2013;129:101–108. URL: https://www.sciencedirect.com/science/article/pii/S0022407313002446. doi:https://doi.org/10.1016/j.jqsrt.2013.05.036.

[67] Drayson, R.. Rapid computation of the voigt profile. J Quant Spectrosc Radiat Transf 1976;16(7):611–614. URL: https://www.sciencedirect.com/science/article/pii/0022407376900297. doi:https://doi.org/10.1016/0022-4073(76)90029-7.

[68] Pierluissi, J.H., Vanderwood, P.C., Gomez, R.B.. Fast calculational algorithm for the Voigt profile. J Quant Spectrosc Radiat Transf 1977;18(5):555–558. URL: https://www.sciencedirect.com/science/article/pii/0022407377900565. doi:https://doi.org/10.1016/0022-4073(77)90056-5.

[69] Zuev, V.. Propagation of laser emission in the atmosphere. Moscow: Publisher: Radio and Communication; 1981.

[70] Laraia, A.L., Gamache, R.R., Lamouroux, J., Gordon, I.E., Rothman, L.S.. Total internal partition sums to support planetary remote sensing. Icarus 2011;215(1):391–

400. URL: https://www.sciencedirect.com/science/article/pii/S0019103511002132. doi:https://doi.org/10.1016/j.icarus.2011.06.004.

[71] Anderson, G.P., Clough, S.A., Kneizys, F.X., Chetwynd, J.H., Shettle, E.P.. AFGL Atmospheric Constituent Profiles (0-120 km). Technical Report Air Force Geophysics Lab Hanscom AFB MA Environmental Research Papers 1986;954:46.

[72] Bürgesser, R.E., Nicora, M.G., Avila, E.E.. Characterization of the lightning activity of "Relámpago del Catatumbo". JASTP 2012;77:241–247. doi:10.1016/j.jastp.2012.01.013.

[73] Makarova, M.V., Kirner, O., Timofeev, Y.M., Poberovskii, A.V., Imkhasin, K.K., Osipov, S.I., et al. Analysis of methane total column variations in the atmosphere near St. Petersburg using ground-based measurements and simulations. Izv - Atmos Ocean Phys 2015;51:177–185. doi:10.1134/S0001433815010089.

[74] Vigouroux, C., Bauer Aquino, C.A., Bauwens, M., Becker, C., Blumenstock, T., De Mazière, M., et al. NDACC harmonized formaldehyde time series from 21 FTIR stations covering a wide range of column abundances. Atmos Meas Tech 2018;11:5049–5073. doi:10.5194/amt-11-5049-2018.